DNS AND RANS SIMULATION OF DISPERSION DOWNSTREAM OF AN OBSTACLE

Riccardo Rossi*, Gianluca Iaccarino**

*Laboratorio di Termofluidodinamica Computazionale, Seconda Facoltà di Ingegneria di Forlì
Università di Bologna, Via Fontanelle 40, 47100 Forlì, Italy

**Center for Turbulence Research, Department of Mechanical Engineering
Stanford University, 488 Escondido Mall, CA 94305, United States

ABSTRACT

Dispersion in the wake of an obstacle is studied as a step towards the analysis of bio-agent release in urban environments. Available experimental measurements are used to compare in details numerical predictions obtained using Reynolds-Averaged Navier-Stokes (RANS) techniques and Direct Numerical Simulations (DNS). In particular, turbulent scalar fluxes are compared to assess the quality of simple closure based on eddy diffusivity assumptions. The results obtained using different RANS closures show considerable spread in the results, with satisfactory agreement obtained by one model which predicts very low levels of turbulence in the obstacle wake. On the other hand, DNS is fairly accurate but very sensitive to adopted inflow conditions. Finally, in terms of the turbulent fluxes the RANS models qualitatively represent the vertical flux but fail to predict the streamwise components while DNS predictions, at least for the highest Reynolds number considered, represent both components with a fairly good level of accuracy.

1 INTRODUCTION AND BACKGROUND

The analysis of scalar dispersion in turbulent flows is relevant to a broad range of applications, including investigation of hazardous releases and reaction capabilities to bioterrorism. In the last fifty years experimental and numerical investigations of canonical flows (Fackrell and Robins, 1982; Livescu et al., 2000) have enhanced theoretical understanding and subsequently enabled the development of simplified, semi-empirical models. Although these models have been successfully employed in simplified flow configurations (Sykes et al., 1984), prediction of scalar dispersion over complex, realistic geometries remains challenging especially because of large-scale unsteady effects which cannot be properly accounted for in a simple phenomenological framework. On the other hand, it is generally accepted that detailed flow simulations (for example Large Eddy Simulation, LES) provide accurate predictions of the turbulence dynamics and the scalar mixing rates, thus promising to enhance our ability to study turbulent dispersion in realistic environments. This in turn could lead to the development of better *reduced-order-models*.
In this paper we present a summary of numerical experiments aimed at establishing the reliability of detailed flow simulations for scalar dispersion predictions in complex geometries (Rossi and Iaccarino, 2008). We initially present a comprehensive Reynolds-Averaged Navier-Stokes based analysis of a reference complex flow (Vinçont et al., 2000) where various *one-point* statistical models - namely $k-\varepsilon$, $k-\omega$ and Reynolds Stress Transport (RST) - are compared to the experimental measurements. As a second step, we performed direct numerical simulations of the same experimental setup with the objective of provide a more detailed analysis of the interaction between turbulence structures and scalar dispersion.

2 PROBLEM DESCRIPTION

The adopted test case consists of the experimental setup of Vinçont et al. (2000), where the scalar dispersion from a line source downstream of a two-dimensional square obstacle has been investigated. The obstacle was completely immersed in a turbulent-boundary layer with an approximate ratio $\delta/h \approx 7$, where δ is the boundary layer thickness previously measured without the obstacle in place and h the obstacle height. The experimental measurements were carried out in a water channel and in a wind tunnel where the flow was characterized by a Reynolds number of 700 and 1500, based on h and the free stream velocity u_∞, and by a Schmidt number of 2500 and 10^{-6} respectively. The scalar was injected in the main flow through a rectangular slot of $0.14h$ width located $1h$ downstream of the obstacle. The flow and the scalar field were subsequently measured at two different streamwise locations: $4h$ and $6h$. Available measured quantities are the following: mean velocity and mean concentration, streamwise and vertical turbulence intensity, Reynolds shear stress and turbulent scalar fluxes. For the details about the measurements techniques the reader is referred to the paper of Vinçont et al. (2000).

3 RANS ANALYSIS

This section summarizes the RANS-based analysis of the experimental test case. The flow governing equations are solved using the finite-volume code FLUENT and further employing three different turbulence models: the standard $k-\varepsilon$ model (Launder and Spalding, 1972), the standard $k-\omega$ model of Wilcox (1998) and a Reynolds Stress

Report Documentation Page

Form Approved
OMB No. 0704-0188

1. REPORT DATE	2. REPORT TYPE	3. DATES COVERED
DEC 2008	**N/A**	**-**

4. TITLE AND SUBTITLE	5a. CONTRACT NUMBER
DNS AND RANS Simulation Of Dispersion Downstream Of An Obstacle	5b. GRANT NUMBER
	5c. PROGRAM ELEMENT NUMBER
6. AUTHOR(S)	5d. PROJECT NUMBER
	5e. TASK NUMBER
	5f. WORK UNIT NUMBER
7. PERFORMING ORGANIZATION NAME(S) AND ADDRESS(ES) **Laboratorio di Termofluidodinamica Computazionale, Seconda Facolt‘a di Ingegneria di Forl‘ý Universit‘a di Bologna, Via Fontanelle 40, 47100 Forl‘ý, Italy**	8. PERFORMING ORGANIZATION REPORT NUMBER
9. SPONSORING/MONITORING AGENCY NAME(S) AND ADDRESS(ES)	10. SPONSOR/MONITOR’S ACRONYM(S)
	11. SPONSOR/MONITOR’S REPORT NUMBER(S)

12. DISTRIBUTION/AVAILABILITY STATEMENT
Approved for public release, distribution unlimited

13. SUPPLEMENTARY NOTES
See also ADM002187. Proceedings of the Army Science Conference (26th) Held in Orlando, Florida on 1-4 December 2008

14. ABSTRACT

15. SUBJECT TERMS

16. SECURITY CLASSIFICATION OF:			17. LIMITATION OF ABSTRACT	18. NUMBER OF PAGES	19a. NAME OF RESPONSIBLE PERSON
a. REPORT **unclassified**	b. ABSTRACT **unclassified**	c. THIS PAGE **unclassified**	**UU**	**8**	

Transport model (Launder et al., 1975). In addition, the one-equation model of Wolfstein (1969) is used to resolve the viscosity-affected near wall region of the flow along with the $k-\varepsilon$ and the RST closures. On the other hand, the $k-\omega$ model already incorporates modifications for low-Reynolds-number effects and is therefore adopted in the outer flow as well as in the near-wall region. The "frozen" velocity field is finally employed in the finite-volume code PS-SOLVER, desgined for the solution of the scalar transport equation in complex geometries (Rossi, 2006, 2008). Therefore, the scalar advection is approximated to a passive mechanism. In this framework, turbulent scalar fluxes are estimated by a standard eddy-diffusivity model assuming a constant turbulent Schmidt number. The numerical model employed in the computations is based on the finite-volume grid shown in Fig. 1, which has an overall resolution of 394×160 in the streamwise and spanwise directions, respectively, while 64×64 cells are placed around the obstacle. Note that a second-order accurate discretization is adopted for both the flow and scalar governing equations, based on upwind-biased reconstruction for advective terms (Barth and Jespersen, 1989). The vertical profiles of

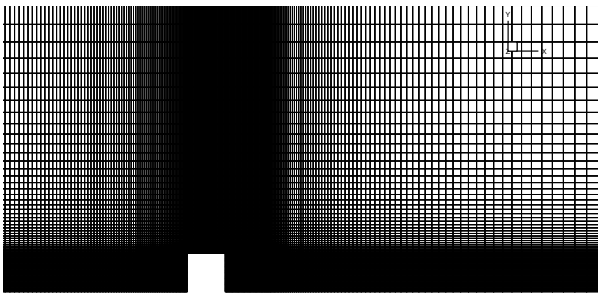

Figure 1. Sketch of the computational grid (Note that only half the grid points are shown for sake of clarity).

mean streamwise velocity are presented in Fig. 2. The results show that the mean flow is fairly well predicted by the RST model for both the water and the air setup. Moreover, while in both cases the $k-\varepsilon$ closure gives a strong underestimation of the separated region downstream of the obstacle, the profiles predicted by the $k-\omega$ model are in better agreement with the experimental measurements. The reattachment lengths given by the three different turbulence closures are summerized in Tab. 1. As suggested by mean velocity profiles, the RST model leads to the best agreement with the experimental results. It is worth noting that although the air setup is characterized by an higher Reynolds number compared to the water setup, the same value of reattachment length has been reported in the experiments. The computed vertical profiles of mean scalar concentration are shown in Fig. 3. The most interesting

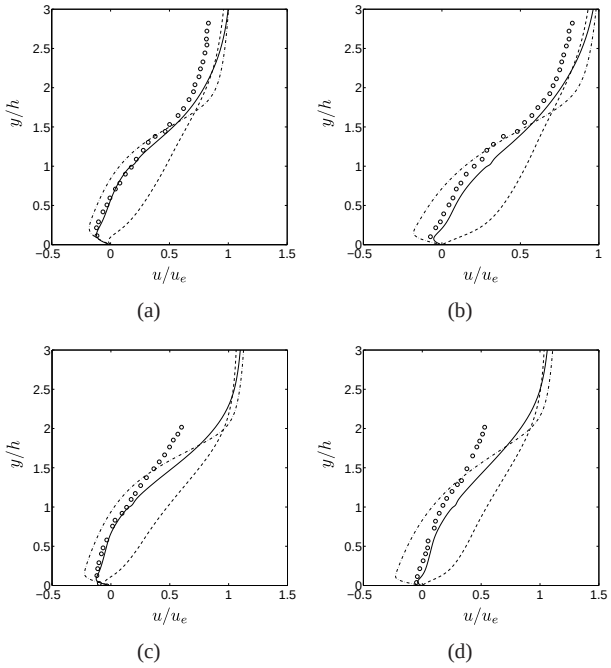

Figure 2. Profiles of mean streamwise velocity: (a) water setup at $x = 4h$, (b) water setup at $x = 6h$, (c) air setup at $x = 4h$, (d) air setup at $x = 6h$; (– – –) $k-\varepsilon$, (– · –) $k-\omega$, (——) RST, (○) Vinçont et al. (2000).

Table 1. Estimated reattachment lengths.

setup	exp	$k-\varepsilon$	$k-\omega$	RST
water	$7h$	$4.55h$	$11.34h$	$7.62h$
air	$7h$	$5.2h$	$9.25h$	$5.65h$

result is that an accurate prediction of local mean velocity profiles does not guarantee a satisfactory prediction of the scalar concentration; the key component is indeed the turbulent scalar diffusivity. This is clearly shown by the comparison of predicted mean concentration profiles given by the $k-\varepsilon$ and RST closures which have a different shape but are almost equivalent in terms of average concentration. They result largely understimated in the water setup, while a closer agreement with the experiments is found at $x = 6h$. Although the $k-\omega$ model gives overall a better agreement with measurements, the results for the air setup suggest a significant influence of the Reynolds number on prediction capability of adopted turbulence closures.

The overall effect of the estimated level of turbulent scalar diffusivity is clearly shown by the contour plots of mean scalar concetration downstream of the obstacle in Fig. 4. A similar scenario to the one described in the work of Vinçont et al. (2000) is predicted, where the scalar is firstly convected upstream and in the vertical direction within the

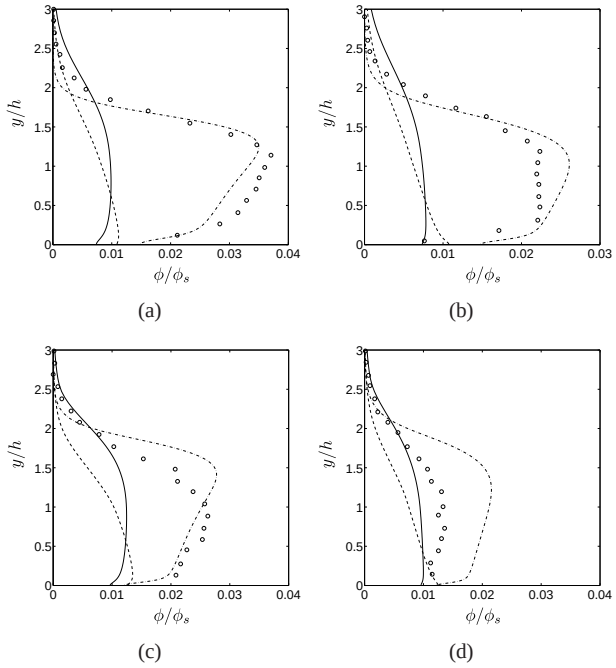

Figure 3. Profiles of mean scalar concentration: (a) water setup at $x = 4h$, (b) water setup at $x = 6h$, (c) air setup at $x = 4h$, (d) air setup at $x = 6h$; (– – –) $k-\varepsilon$, (– · –) $k-\omega$, (——) RST, (○) Vinçont et al. (2000).

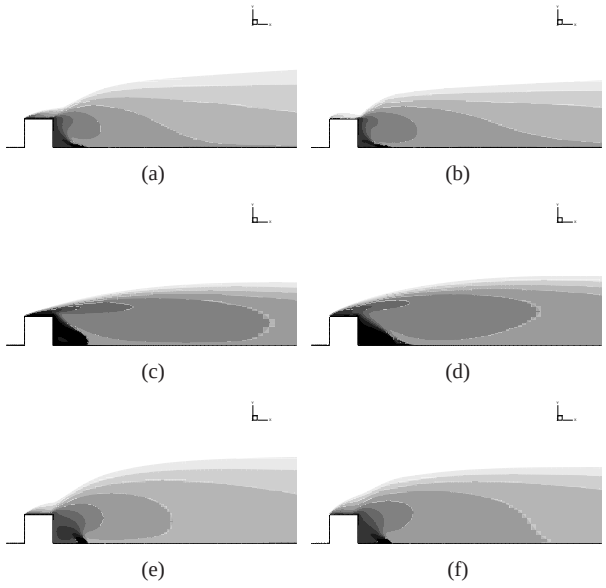

Figure 4. Mean scalar concentration downstream of the obstacle: (left-column) water setup, (right-column) air setup; (a,b) $k-\varepsilon$, (c,d) $k-\omega$, (e,f) RST; contours range is 0.001-0.9.

flow reversal region to fill the separation bubble over the top of the body, before being convected downstream by the primary flow. Therefore, each one of adopted turbulence models are able to capture the salient features of the mean flow: the large flow reversal region behind the body and the smaller separation bubble above the obstacle. However, a different size of the scalar wake is highlighted in the contour plots. As expected, the $k-\varepsilon$ and the RST closures yield a larger wake, suggesting a stronger diffusive flux across the wake boundary. Moreover, although the RST model gives a better representation of the wake development, both turbulence closures give rise to a sharp decrease of the scalar concentration after the injection into the main flow. It is clear by looking to the results in Fig.s 4(c) and 4(d) that this is not the case when the $k-\omega$ model is employed, where the scalar concentration is almost uniform in the region of flow reversal close to the body. Futhermore, a higher concentration is predicted in the shear layer above the obstacle, which finally results in the development of a confined scalar wake.

The profiles of turbulent scalar fluxes at $x = 4h$ are finally presented in Fig. 5. A reasonable agreement with the experimental data is found for the $k-\omega$ model, which is able to partially match the location and magnitude of local extrema of the vertical component, while no one of adopted turbulence closures is able to predict the streamwise flux. Since it has been shown that the $k-\omega$ model gives a reliable estimation of mean scalar concentration, it might be concluded that the net contribution of the streamwise component in the scalar transport equation is negligeable. It is worth outlining that the experiments show a very strong negative streamwise flux within the shear layer at $y/h \approx 2$. This region does not correspond to negative velocity (at $x/h = 4$ the reverse flow is confined to $y/h < 0.75$) and therefore corresponds to an actual *anti-diffusion* mechanism.

4 DNS ANALYSIS

The DNS-based analysis of the experimental setup are carried out with the objective of providing a more detailed analysis of the interaction between turbulent structures and scalar dispersion. The numerical solution of the Navier-Stokes and scalar transport equations is obtained using second-order accurate finite-volume techniques and a block-hexahedral grid. In this framework, the presence of the obstacle is easily managed by employing an unstructured grid connectivity. However, the most critical issue in the analysis of spatially-developing flows using direct and large-eddy simulations is represented by inflow and outflow boundary conditions. While it is generally accepted that convective boundary conditions at the outlet of the computational domain are suitable to the analysis of incompressible flows, it has been clearly established that inflow conditions can strongly affect the downstream development of the flow field (Le and Moin, 1992). Therefore, in the present analysis two different boundary settings are con-

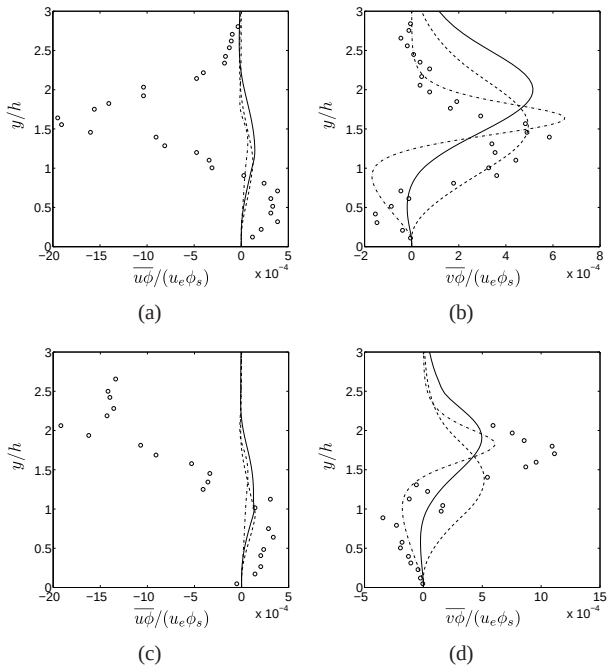

Figure 5. Profiles of turbulent scalar fluxes: (a) streanwise component of water setup, (b) vertical component of water setup , (c) streamwise component of air setup, (d) vertical component of air setup; (– – –) $k-\varepsilon$, (–·–) $k-\omega$, (——) RST, (○) Vinçont et al. (2000).

sidered:

1. Constant velocity profile/zero-fluctuations (Uniform inflow)
2. Boundary layer profile/superimposed fluctuations (Turbulent inflow)

In both cases the flow is supposed homogeneous in the spanwise direction, where a periodic condition is applied, while a slip condition is employed at the upper boundary of the computational domain. The spatial extent of the computational domain is $35h \times 15h \times 8h$ while the overall grid resolution in wall units is reported in Tab. 2. The code

Table 2. Spatial extent of the computational domain and grid resolution in wall units.

setup	size	Δx^+	Δy^+	Δz^+
water	$229 \times 80 \times 32$	$1.2-38.2$	$1.2-30.6$	9.5
air	$229 \times 80 \times 32$	$2.3-73.3$	$2.3-58.6$	18.2

CDP (Mahesh et al., 2004) is adopted in the analysis of the uniform inflow condition while the turbulent inflow simulation is performed with the help of the FLUENT code. The specification of the turbulent inflow is based on the random flow generation technique originally proposed by Kraichnan (1970) and modified later by Smirnov et al. (2001). Note that both codes adopt the fractional step method for the pressure-velocity coupling and a low-order central interpolation scheme (LO-CD) for advective terms to guarantee the conservation of kinetic energy and therefore the numerical stability (Felten and Lund, 2006).

At each time step, the continuity-satisfying mass flow rates are employed at cell faces to solve the scalar transport equation. For the grid resolution adopted in this initial validation of the numerical technique, the very sharp gradients arising at the edge of the scalar wake are such that upwind-biased schemes cannot be avoided to achieve numerical stability. Therefore, in the CDP code the QUICK scheme of Leonard (1979) is adopted for the dicretization of advective terms. In the case of the PS-SOLVER, a second-order accurate upwind scheme (SOU) based on the *slope-limiter* technique originally introduced by Van Leer (1974) and subsequently extended to unstructured grids by Barth & Jespersen (1989) is employed. A null-flux condition is finally specified at the solid boundaries while a uniform scalar injection (i.e. a constant profile without superimposed fluctuations) is assumed at the slot.

An initial condition of a zero-velocity field and zero-concentration of the contaminant is employed. The solution is then advanced in time using a non-dimensional time-step size $\Delta t^+ = u_\tau \Delta t/h$ of 1.862×10^{-3} and 7.623×10^{-4} for the water and the air setup, respectively, until an approximate statistically steady-state is reached. At this point, turbulence statistics are computed over a time interval of 186 $u_\tau t/h$ for the case of water and 90 $u_\tau t/h$ for the air setup.

4.1 Uniform inflow

In this section the results obtained from the analysis of the uniform inflow condition are presented. For sake of completeness the computations have been carried out using both the CDP code and the FLUENT/PS-SOLVER package, while the results previously obtained using the $k-\omega$ model are also reported to allow a direct comparison. Note that the RANS-based analysis has been performed by specifying a boundary layer profile at the inflow.

The vertical profiles of mean streamwise velocity are shown in Fig. 6. Although the separated regions are clearly overstimated in both the numerical experiments, in the case of the water setup the shape of the velocity profile is also very different from measurements: at $x = 4h$ the flow is nearly stagnant within the recirculating region, while at $x = 6h$ the backflow velocity is almost constant up to the location of the shear layer ($y \approx 1.5h$). The results obtained by the CDP and the FLUENT code are almost identical. The situation is considerably different in the air setup, where the backflow velocity is not consistently computed using

the two codes. This result indicates that the different numerical techniques adopted in the two codes affect the predictions of turbulent structures. It is also interesting to note that the velocity at the edge of the profile is largely affected by the uniform inflow, being strongly overpredicted compared to both the reference datasets. The computed mean

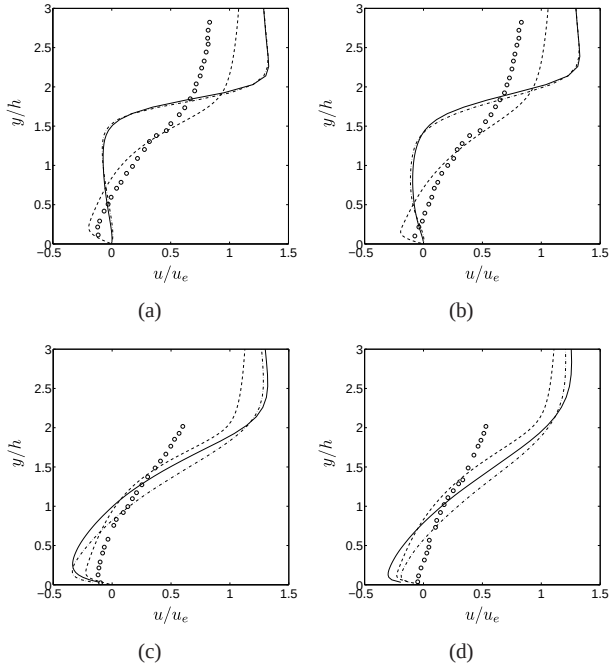

Figure 6. Profiles of mean streamwise velocity for the uniform inflow condition: (a) water setup at $x = 4h$, (b) water setup at $x = 6h$, (c) air setup at $x = 4h$, (d) air setup at $x = 6h$; (– – –) $k-\omega$, (–·–) FLUENT, (——) CDP, (○) Vinçont et al. (2000).

scalar profiles are presented in Fig. 7. It is clear from the analysis of the water setup in Fig.s 7(a) and 7(b) that turbulent dispersion is nearly absent at both streamwise locations. This is suggested by the local peak of scalar concentration within the shear-layer ($y \approx 1.5h - 2h$), which is very similar to the laminar profile that would be obtained in the limit of $Sc, Sc_t \to \infty$ using RANS models. Therefore, in the case of the water setup the scalar dispersion is dominated by the mean flow transport. This is also confirmed by the constant scalar concentration within the obstacle height ($y < 1h$) where the flow is nearly stagnant (see Fig.s 6(a) and 6(b)). The concentration profiles also show the more diffusive character of the upwind discretization adopted in the code PS-SOLVER compared to the QUICK scheme employed in the CDP code. In the air setup, the concentration is finally underpredicted (see Fig.s 7(c) and 7(d)) and the absence of high concentration in the shear-layer indicates the presence of a stronger turbulent scalar flux in the vertical direction.

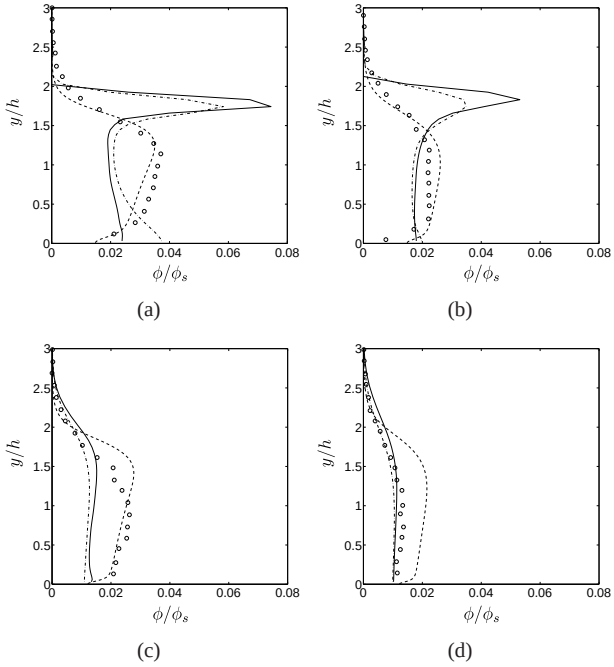

Figure 7. Profiles of mean scalar concentration for the uniform inflow condition: (a) water setup at $x = 4h$, (b) water setup at $x = 6h$, (c) air setup at $x = 4h$, (d) air setup at $x = 6h$; (– – –) $k-\omega$, (–·–) FLUENT, (——) CDP, (○) Vinçont et al. (2000).

4.2 Turbulent inflow

The analysis of the results obtained by adopting the uniform inflow clearly suggests a strong influence on the development of the scalar wake, determined by the onset of transition in the shear-layer developing from the leading edge of the square obstacle. Therefore, in this section the analysis is focused on the effect of the turbulent inflow condition described at the beginning of Section 4. The computations are performed using the FLUENT/PS-SOLVER package and the results will be directly compared to those obtained from the uniform inflow analysis.

A first insight into the effect of introducing randomly generated turbulent fluctuations at the inflow is given in Fig. 8. In the case of the water setup the breakdown of the shear-layer occurs closer to the obstacle; the region above the scalar source is characterized by larger fluctuations. On the other hand in the air setup the opposite behavior is observed, with the shear-layer becoming more regular. In the water setup, the boundary layer approaching the obstacle changes the inception of the shear layer and, as it has been shown by Zhuang (1999), produces an increased streamlines curvature which is destabilizing. On the other hand

in the air setup the velocity profile at the inlet results in a lower velocity at the obstacle height, and therefore in a more stable shear layer. The analysis of mean velocity pro-

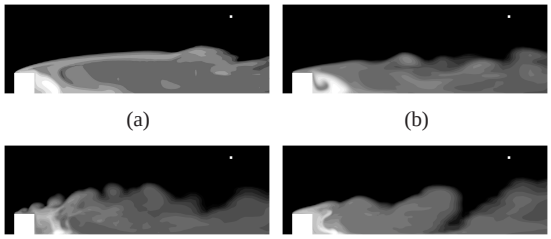

Figure 8. Instantaneous scalar wake structure downstream of the square obstacle in the fully developed regime: (a) water setup with uniform inflow, (b) water setup with turbulent inflow, (c) air setup with uniform inflow, (d) air setup with turbulent inflow.

files in Fig. 9 shows that the turbulent inflow condition has a dominant effect on computed first-order statistical moments for the water setup. The early stage of transition occuring closer to the obstacle causes a significant change in the profiles shape, particularly at $x = 6h$. Furthermore, the adoption of the boundary layer profile at the inlet of the computational domain yields a very large velocity reduction at the edge of the boundary layer, giving a closer agreement with the experiments. However, the region of flow reversal is still strongly overstimated. In the case of the air setup the present profiles confirm the early transition of the shear-layer even in the absence of fluctuations at the inlet section, the profiles shape being very similar between the uniform and turbulent inflow conditions. This suggests that the turbulent transport is active in both cases. Note that as in the case of the water setup the outer velocity in Fig.s 9(c) and 9(d) is significantly reduced by adopting the boundary layer profile at the inflow, but the separated region is still overpredicted. The analysis of the Reynolds stress $\overline{uv}$ in Fig. 10 shows that the profiles are consistent with the scenario depicted for the mean velocity field. In the case of the water setup the turbulent transport at $x = 4h$ is practically absent when the uniform inflow is employed, indicating that streamwise and vertical turbulent fluctuations are not correlated. If the turbulent inflow is activated a significant contribution is present across the shear-layer, while it is nearly zero up to the obstacle height. This is again in agreement with the small change in the mean velocity profile shown in Fig. 9(a). The flow conditions at $x = 6h$ are similar; the turbulent transport is significantly larger in the case of the turbulent inflow within the obstacle size, resulting in the different shape of the velocity profile in Fig. 9(b). The Reynolds stress profiles for the air setup in Fig.s 10(c) and 10(d) suggest once again the damping ef-

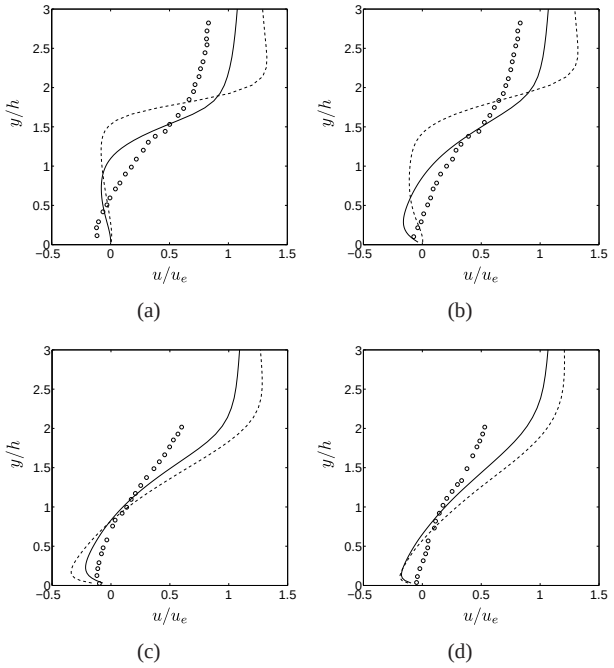

Figure 9. Profiles of mean streamwise velocity: (a) water setup at $x = 4h$, (b) water setup at $x = 6h$, (c) air setup at $x = 4h$, (d) air setup at $x = 6h$; (– – –) uniform inflow, (——) turbulent inflow, (○) Vinçont et al. (2000).

fect following from the boundary layer profile with superimposed fluctuations at the inlet. At both streamwise locations, a significant reduction of the correlation between the fluctuations of velocity components is found. The results for the mean scalar concentration are presented in Fig. 11. The profiles shape for the water setup are closely related to the mean velocity field shown in Fig.s 9(a) and 9(b). At $x = 4h$ the effect of the turbulent inflow is not particularly evident and the profile is just shifted downward in the vertical direction. Moreover, a sharp increase of the scalar concentration close to $y \approx 1.5h$ is found using both inflow conditions. In spite of that, the earlier onset of transition in the case of the turbulent inflow can be noted at $x = 6h$, where the mean scalar profile is in closer agreement with the reference dataset. On the other hand, as it can be noted in Fig.s 11(c) and 11(d), the overall effect of the fluctuations at the inlet is clear at both the streamwise locations for the air setup. The predicted profiles are consistent with the reduced level of turbulent velocity fluctuations, resulting in the higher scalar concentration compared to the uniform inflow results. However, while the agreement with the experimental measurements is satisfactory at $x = 4h$, the profile obtained at $x = 6h$ is overestimated. The analysis of turbulent scalar fluxes for the water setup in Fig.s 12(a) and 12(b) shows a significant improvement in the computed profiles when the turbulent inflow is employed. Moreover, while

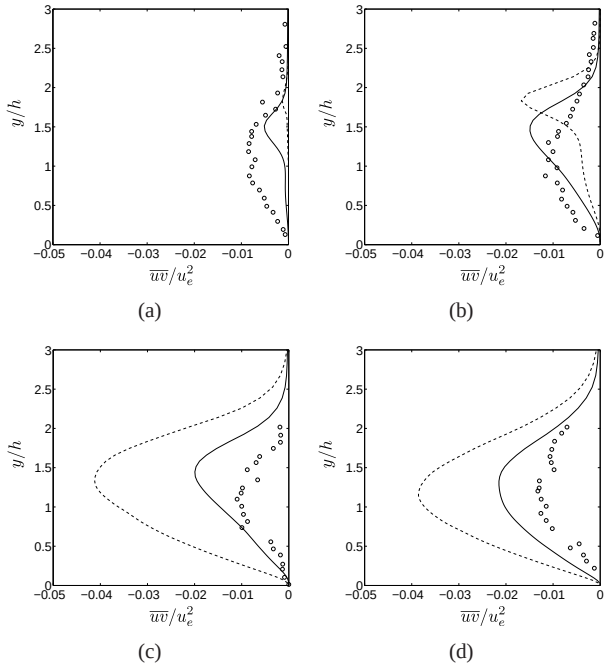

Figure 10. Profiles of Reynolds stress $\overline{uv}$: (a) water setup at $x = 4h$, (b) water setup at $x = 6h$, (c) air setup at $x = 4h$, (d) air setup at $x = 6h$; (– – –) uniform inflow, (——) turbulent inflow, (○) Vinçont et al. (2000).

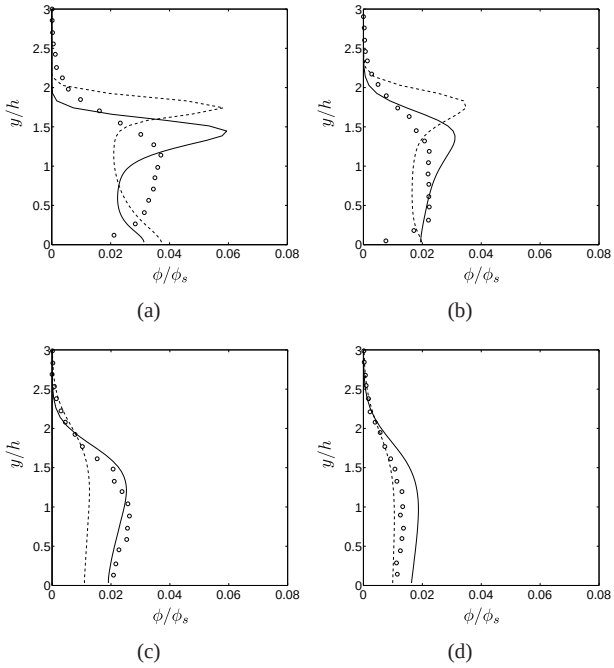

Figure 11. Profiles of mean scalar concentration: (a) water setup at $x = 4h$, (b) water setup at $x = 6h$, (c) air setup at $x = 4h$, (d) air setup at $x = 6h$; (– – –) uniform inflow, (——) turbulent inflow, (○) Vinçont et al. (2000).

a vanishing streamwise component has been predicted by RANS-based models, both the magnitude and location of the negative peak are reasonably reproduced by the present computations. Nonetheless, the weak positive peak is overpredicted and shifted upward in the vertical direction compared to the experimental measurements. The results also show that the vertical component is far from the reference dataset, while a better agreement for turbulent scalar fluxes is found for the air setup in Fig.s 12(c) and 12(d). This scenario is in agreement with the results for the mean scalar profile at the same streamwise location (see Fig.s 9(a) and 9(c)), showing that accurate predictions of turbulent transport have a crucial role in high-fidelity simulations of scalar dispersion.

5 CONCLUSIONS

A preliminary study of scalar dispersion downstream of a square obstacle has been presented as a step towards the analysis of bio-agent release in urban environments. The comparison with available experimental measurements has shown that the scalar concentration given by RANS-based models is dominated by the predicted eddy-diffusivity. Although the $k-\omega$ model has been able to give a good agreement for the water setup, the analysis of the air setup also indicates that the predictive capability of the model are Reynolds number dependent. On the other hand, DNS yield greater reliability in the comparison with experimental results but has been found very sensitive to adopted inflow conditions. However, the results clearly show that DNS are able to properly evaluate both the streamwise and vertical components of turbulent scalar fluxes. Therefore, the present work suggests that high-fidelity simulations can be a promising tool in the analysis of scalar dispersion in complex geometries.

ACKNOWLEDGMENTS

The authors acknowledge the High Performance Computing Center at Stanford University for providing computing resources that have contributed to the research results presented in this paper. The support from the Stanford AHPCRC is also gratefully acknowledged.

REFERENCES

Fackrell, J. E. and Robins, A. G., 1982: Concentration fluctuations and fluxes in plumes from point sources in a turbulent boundary layer, *J. Fluid Mech.*, **117**, 1-26.

Livescu, D., Jaberi, F. A. and Madnia, C. K., 2000: Passive-scalar wake behind a line source in grid turbulence, *J. Fluid Mech.*, **416**, 117-149.

Sykes, R. I., Lewellen, W. S. and Parker, S. F., 1984:

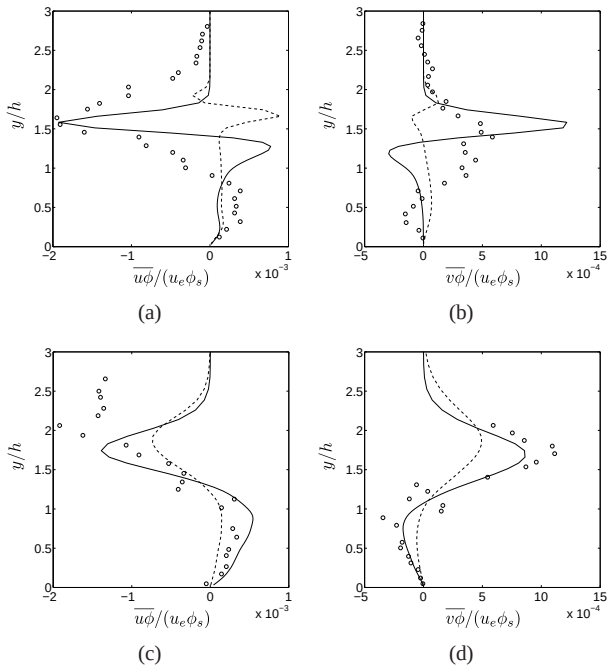

Figure 12. Profiles of turbulent scalar fluxes for the water setup; (a) streamwise component of water setup, (b) vertical component of water setup, (c) streamwise component of air setup, (d) vertical component of air setup; (– – –) uniform inflow, (——) turbulent inflow, (○) Vinçont et al. (2000).

A turbulent-transport model for concentration fluctuations and fluxes, *J. Fluid Mech.*, **139**, 193-218.

Rossi, R. and Iaccarino, G., 2008: Numerical simulation of scalar dispersion downstream of a square obstacle, Technical Report RR/GI/08, Center for Turbulence Research, Stanford University.

Vinçont, J.-Y., Simöens, S. , Ayrault, M. and Wallace, M., 2000: Passive scalar dispersion in a turbulent boundary layer from a line source at the wall and downstream of an obstacle, *J. Fluid Mech.*, **424**, 127-167.

Launder, B. E. and Spalding, D. B., 1972: Lectures in mathematical models of turbulence, Academic Press, London.

Wilcox, D. C., 1998: Turbulence Modeling for CFD, DCW Industries Inc., La Canada, California.

Launder, B. E., Reece, G. J. and Rodi, W., 1975: Progress in the development of a Reynolds-stress turbulence closure, *J. Fluid Mech.*, **68**, 537-566.

Wolfstein, M., 1969: The velocity and temperature distribution of one-dimensional flow with turbulence augmentation and pressure gradient, *Int. J. Heat Mass Transfer* **12**, 301-318.

Rossi, R., 2006: Passive scalar transport in turbulent flows over a wavy wall, PhD Thesis, Università degli Studi di Bologna.

Rossi, R., 2008: Direct numerical simulation of scalar transport using unstructured finite-volume schemes, Accepted as a publication in the Journal of Computational Physics.

Barth, T. J. and Jespersen, D., 1989: The design and application of upwind schemes on unstructured meshes, Technical Report AIAA-89-0366, AIAA 27th Aerospace Sciences Meeting, Reno, Nevada.

Le, H. and Moin, P., 1992: Direct numerical simulation of turbulent flow over a backward-facing step, *Annual Research Briefs*, Center for Turbulent Research, Stanford University and NASA-Ames, 161-173.

Mahesh, K., Constantinescu, G., and Moin, P., 2004: A numerical method for large-eddy simulation in complex geometries, *J. Comput. Phys.*, **197**, 215-240.

Kraichnan, R., 1970: Diffusion by a random velocity field, *Phys. Fluids*, **11**, 21-31.

Smirnov, R., Shi, S. and Celik, I., 2001: Random flow generation technique for large eddy simulations and particle-dynamics modeling, *J. Fluids Eng.*, **123**, 359-371.

Felten, F. N. and Lund, T. S., 2006: Kinetic energy conservation issues associated with the collocated mesh scheme for incompressible flow, *J. Comput. Phys*, **215**, 465-484.

Leonard, B. P., 1979: A stable and accurate convective modelling procedure based on quadratic upstream interpolation, *Comp. Methods Appl. Mech. Eng.*, **19**, 59-98.

Van Leer, B., 1974: Towards the ultimate conservative difference scheme II. Monotonicity and conservation combined in a second order scheme, *J. Comp. Phys.*, **14**, 361-370.

Zhuang, M., 1999: The effect of curvature on wake-dominated incompressible free shear layers, *Phys. of Fluids*, **11**, 3106-3115.